Article

Investigating the Performance of Red and Far-Red SIF for Monitoring GPP of Alpine Meadow Ecosystems

Weina Duan [1,2], Xinjie Liu [2,3,*], Jidai Chen [2,3], Shanshan Du [2,3], Liangyun Liu [2,3] and Xia Jing [1]

[1] College of Geomatics, Xi'an University of Science and Technology, Xi'an 710054, China; 20210061037@stu.xust.edu.cn (W.D.); jingxia@xust.edu.cn (X.J.)
[2] Key Laboratory of Digital Earth Science, Aerospace Information Research Institute, Chinese Academy of Sciences, Beijing 100094, China; chenjidai@aircas.ac.cn (J.C.); duss@radi.ac.cn (S.D.); liuly@radi.ac.cn (L.L.)
[3] International Research Center of Big Data for Sustainable Development Goals, Beijing 100094, China
* Correspondence: liuxj@radi.ac.cn

Abstract: Alpine meadow ecosystems are extremely vulnerable to climate change and serve an essential function in terrestrial carbon sinks. Accurately estimating their gross primary productivity (GPP) is essential for understanding the global carbon cycle. Solar-induced chlorophyll fluorescence (SIF), as a companion product directly related to plant photosynthesis process, has become an attractive pathway for estimating GPP accurately. To date, the quantitative SIF-GPP relationship in terrestrial ecosystems is not yet clear. Especially, red SIF and far-red SIF present differences in their ability to track GPP under different environmental conditions. In this study, we investigated the performance of SIF at both red and far-red band in monitoring the GPP of an alpine meadow ecosystem based on continuous tower-based observations in 2019 and 2020. The results show that the canopy red SIF (SIF_{Red}) and far-red SIF ($SIF_{Far-red}$) were both strongly correlated with GPP. SIF_{Red} was comparable to $SIF_{Far-red}$ for monitoring GPP based on comparisons of both half-hourly averaged and daily averaged datasets. Moreover, the relationship between SIF_{Red} and GPP was linearly correlated, while the relationship between $SIF_{Far-red}$ and GPP tended to be nonlinear. At a diurnal scale, dramatic changes in photosynthetically active radiation (PAR), air temperature (Ta), and vapor pressure deficit (VPD) all had effects on the slope of the linear fitted line with zero intercept for SIF_{Red}-GPP and $SIF_{Far-red}$-GPP, and the effect on the slope of the linear fitted line with zero intercept for $SIF_{Far-red}$-GPP was obviously stronger than that for SIF_{Red}-GPP. PAR was the dominant factor among the three environmental factors in determining the diurnal variation of the slope of SIF-GPP. At a seasonal scale, the $SIF_{Far-red}$/GPP was susceptible to PAR, Ta, and VPD, while the SIF_{Red}/GPP remained relatively stable at different levels of Ta and VPD, and it was only weakly affected by PAR, suggesting that SIF_{Red} was more consistent than $SIF_{Far-red}$ with GPP in response to seasonal variations in environmental factors. These results indicate that SIF_{Red} has more potential than $SIF_{Far-red}$ for monitoring the GPP of alpine meadow ecosystems and can also assist researchers in gaining a more comprehensive understanding of the diversity of SIF-GPP relationships in different ecosystems.

Keywords: alpine meadow; solar-induced chlorophyll fluorescence (SIF); gross primary production (GPP); tower-based observation

1. Introduction

Alpine meadow is a typical alpine ecosystem found globally and consists of hardy perennial herbaceous communities, and such meadows are mainly distributed at high altitudes and covers about one-third of the Qinghai–Tibet Plateau (QTP). They have a crucial role in the carbon cycle and serve as an essential ecological security barrier in alpine regions [1–3]. Alpine meadows of the QTP are exposed to intensive and sufficient solar radiation throughout the year, including strong ultraviolet radiation [4]. Temperatures at the QTP usually undergo wide diurnal variation, and the temperature and rainfall

here are severely influenced by latitude, topography, and atmospheric circulation, making the growing environment of alpine meadows extremely harsh [3]. Previous studies have demonstrated the vulnerability of alpine ecosystems to major changes in climate [3,5–7], which inevitably leads to changes in carbon fluxes in this ecosystem [4].

Gross primary productivity (GPP) is the sum of total organic carbon fixation through photosynthesis within the vegetation under natural light conditions, which is an important indicator of carbon fluxes [8–10]. Accurate estimations of the GPP of ecosystems is important for understanding the state of the ecosystem response to environmental variations and changes in carbon balance [11,12]. Throughout recent decades, an increasing number of researchers have become accustomed to utilizing solar-induced chlorophyll fluorescence (SIF) as a promising approach on monitoring GPP [11,13,14]. SIF is an emission spectrum showing two emitting peaks in the red and far-red bands, which is a by-product of the photosynthesis process [11,15–17]. Thereby, SIF is directly related to photosynthesis and could be treated as an indicator of GPP [15,18–21].

Most current studies on the association of SIF and GPP have focused on cropland, forest, grassland, and wetland ecosystems, and SIF-based GPP monitoring has demonstrated a strong ability to track changes in all of these ecosystems. Canopy far-red SIF ($SIF_{Far-red}$) follows likeness seasonal and diurnal pattern of variation to GPP, which have been observed in crops [14,22–25], forests [26–28], and coastal salt marsh ecosystems [29]. In crop ecosystems such as wheat, maize, rice, and soybean, many studies have found that $SIF_{Far-red}$ showed an obvious linear relationship with GPP [24,25,30,31], but this linear relationship is highly variable depending on the type of crop photosynthetic pathway [24]. Additionally, studies on grassland ecosystems based on the GOME-2 terrestrial chlorophyll fluorescence data product and FLUXNET GPP data have shown good linear relationships between $SIF_{Far-red}$ and GPP in multi-year data on monthly time scales but also variations in the correlations between $SIF_{Far-red}$ and GPP due to differences in the types of photosynthetic pathways of grasslands [32,33]. Several studies on evergreen coniferous [26], evergreen broadleaf [34], and deciduous broadleaf forests [35] have shown that, under normal growth conditions, $SIF_{Far-red}$ exhibited a positive linear relationship with GPP at different time scales, although the coefficient of determination (R^2) of this linear relationship varied obviously depending on the observed time scale. More recently, a study on coastal salt marsh ecosystems also reported that $SIF_{Far-red}$ had an obvious linear correlation with GPP in coastal salt marsh ecosystems, and the linearity strengthened with increasing time scale [29]. However, other studies have also revealed that $SIF_{Far-red}$ and GPP have a nonlinear relationship. For example, Chen et al. [23] found a hyperbolic relationship between maize $SIF_{Far-red}$ and GPP. The results from a study on evergreen coniferous forests showed a strong nonlinear relationship between $SIF_{Far-red}$ and GPP on both diurnal and seasonal scales, mainly because the GPP was saturated with increasing absorbed photosynthetically active radiation (APAR), while $SIF_{Far-red}$ was not [36]. Another study demonstrated that the linear correlation for $SIF_{Far-red}$ with GPP shifted from positive to negative when the trees were subjected to extreme weather conditions (e.g., heat waves) in evergreen broadleaf forests, thus showing an overall nonlinear correlation [34]. This is mainly due to a change in internal plant energy allocation as an evergreen broadleaf forest experiences nonphotochemical quenching (NPQ) saturation and continuous photoinhibition during heat waves [34].

Notably, researchers prefer to use $SIF_{Far-red}$ to study the dynamics of GPP in various ecosystems [14], owing to the fact that fluorescence in the red band is strongly influenced by reabsorption, and that accurate retrieval of SIF is easier in the far-red than the red band. Benefiting from the improvement of signal-to-noise ratio and spectral resolution of spectral measurement instruments, as well as the development of fluorescence inversion algorithms, researchers have also explored the relationship between canopy red SIF (SIF_{Red}) and GPP [37]. For instance, through downscaling from the observed canopy level SIF to the photosystem level in maize, Liu et al. [38] investigated the relationship between photosystem level SIF and GPP in maize. As compared to canopy-level red SIF, the correlation between photosystem-level red SIF and GPP was found to be greatly enhanced and even

better than that between photosystem-level far-red SIF and GPP. During the wheat canopy growth stage, the correlation between $SIF_{Far-red}$ and GPP was found to be stronger than that between SIF_{Red} and GPP [14]. When the growing stage reached a stable state, $SIF_{Far-red}$ was slightly weakened in relation to GPP, while SIF_{Red} was strengthened in relation to GPP, thereby causing the correlations between SIF_{Red} and GPP and between $SIF_{Far-red}$ and GPP to be comparable [14]. Magney et al. [26] studied on an evergreen coniferous forest and stated that the expected increase in SIF_{Red} did not occur as a consequence of the absence of a significant increase in chlorophyll concentration, and that SIF_{Red} was capable of closely tracking the seasonal changes in GPP in this evergreen coniferous forest.

Across various environmental conditions, the relationship is by no means invariant between SIF and GPP. Previously, an investigation on mangroves showed that VPD negatively affected the strength of the SIF-GPP relationship in mangroves, and that the SIF-GPP correlation did not consistently get stronger as PAR and air temperature increased. The strength of the SIF-GPP relationship in mangroves was most strongly correlated at moderate PAR and air temperature. Thereby high PAR, air temperature, and VPD would weaken the correlation between SIF-GPP in mangrove ecosystem [39]. Yang et al. [25] exhibited that variations in relative humidity and temperature had obvious effects on the ratio of GPP to $SIF_{Far-red}$ for rice. At the same humidity level, the ratio of GPP to $SIF_{Far-red}$ diminished with elevated temperature, while at the same temperature level, the ratio of GPP to $SIF_{Far-red}$ showed an increase with elevated relative humidity. In a subalpine coniferous forest ecosystem, Yang et al. [40] found that there were differences in the relative importance of environmental factors driving changes in GPP and SIF_{Red} from spring to winter. Moreover, SIF_{Red} responded to light earlier than GPP after winter dormancy ends, potentially making it challenging to capture the onset of the photosynthetic season using SIF_{Red}. Regarding a coastal salt marsh ecosystem, tidal inundation had a negative effect on the relationship between $SIF_{Far-red}$ and GPP, mainly due to its different degrees of effects on the light use efficiency (LUE), fluorescence escape probability, and fluorescence quantum yield of vegetation in coastal salt marshes, which affected the performance of $SIF_{Far-red}$ in accurately estimating GPP [29]. Across global scales, Chen et al. [41] showed that moisture availability had a remarkable moderating effect on the SIF-GPP relationship and that the most important environmental factors influencing the SIF-GPP relationship differed in diverse climatic zones. Furthermore, Chen et al. [42] focused on the Northern Hemisphere SIF-GPP relationship and found that the seasonal variation in the SIF-GPP relationship was strongest in regions of moderate temperature and precipitation. Evidently, the effects of environmental factors on the SIF-GPP relationship display different patterns in different regions, making it very essential to consider the transformation of the SIF-GPP relationship at different levels of various environmental factors.

Although advances have been made in the SIF-GPP relationship and its response to environmental factors in some ecosystems, apparently the SIF-GPP relationship varies with ecosystem shifts. Even in the same ecosystem, the SIF-GPP relationship varies significantly due to the different stages of vegetation growth and the effects of changes in different environmental factors on vegetation. The SIF-GPP relationship in the whole terrestrial ecosystem is not clarified, therefore, it is necessary to investigate the SIF-GPP relationship under different ecosystems and the influence of environment on this relationship. However, for some special ecosystems, such as alpine meadow, there has rarely been research on how SIF and GPP relate to each other and the effects of environmental factors on their relationships. Furthermore, since researchers investigated the relationship between $SIF_{Far-red}$ and GPP much more frequently than the relationship between SIF_{Red} and GPP in various ecosystems, this has resulted in the scarcity of information on diurnal and seasonal variations of SIF_{Red} and SIF_{Red}-GPP relationships in various ecosystems. However, SIF_{Red}, mainly generated from photosystem II, reveals more information related to plant physiological changes than $SIF_{Far-red}$ and, therefore, has theoretically more potential for the accurate monitoring of GPP [14,15,20,43].

We are aware of still no research on the use of tower-based continuous observations to study SIF-GPP relationships for alpine meadow ecosystems. Hence, in this study, we collected canopy reflectance spectral data, SIF spectral data, meteorological variables data, and carbon flux data of alpine meadows for two growing seasons using a continuous automatic tower-based observation system. Based on the above observations, our main research objectives are to investigate that for alpine meadow ecosystem, (1) whether SIF at red and far-red bands could track variations of GPP over diurnal and seasonal scales; (2) what is the effect of environmental factors upon the SIF-GPP relationship for different bands; and (3) whether the SIF-GPP relationship and its environmental effects are wavelength-dependent and which band is better for GPP estimation.

2. Materials and Methods

2.1. Experimental Site

Long-term continuous in-situ spectral measurements based on tower-based observations were conducted in 2019 and 2020 at the Arou (AR) site, a grassland site (Figure 1) in the ChinaSpec network, a ground-based continuous SIF observation network of flux tower sites in China [44]. The AR site was also established for use in the Heihe Watershed Allied Telemetry Experimental Research (HiWATER) experiment [45]. The AR site is located in Arou Township, Qilian County, Qinghai Province, Western China (100.4643E, 38.0473N, altitude 3033 m), and in the hinterland of the middle Qilian Mountains in the northeastern region of the Qinghai–Tibet Plateau, with a typical plateau continental climate [5]. The average multi-year temperature is around 0.7 °C, the average yearly precipitation is 400 mm, and the yearly snowfall period reaches about 240–270 days, with absence of absolute frost-free period all year round. The underlying surface of the AR site is mainly alpine meadow. The grass can reach heights of 30 cm during the peak growing period in summer. With high atmospheric transparency, thin air, strong solar radiation, long illuminating hours, and abundant incoming radiation throughout the year, SIF and GPP relationship for alpine meadow may, to some extent, differ from those of other ecosystems.
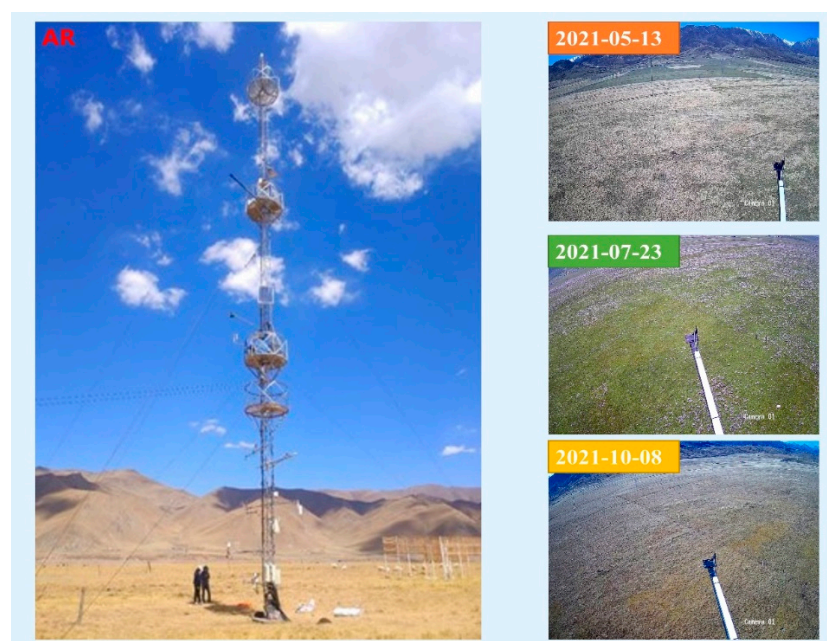

Figure 1. AR's observation tower and pictures of the alpine meadow in spring, summer, and autumn captured by the camera mounted above the tower.

2.2. Tower-Based Spectral Measurements

An automated long term in-situ SIF observation system, SIFSpec, was installed on a tower-based platform about 17 m from the ground for continuous SIF spectral measure-

ments [44,46]. The main components of the SIF observation system include (1) a customized Ocean Optics QE65 Pro spectrometer (Ocean Optics, Dunedin, FL, USA) with a spectral range of 649–805 nm, a spectral resolution of 0.34 nm, a sampling interval of 0.155 nm, and a signal-to-noise ratio (SNR) of >1000 [46]; (2) a computer storing the spectral data and information about the instrument operation status and a software control system controlling the switching of instrument switches and electronic switches [46]; (3) a Y-shaped bifurcated optical fiber (CPATCH, Ocean Optics, Inc., Dunedin, FL, USA), two five meters long optical fibers (core diameter 1000 μm); (4) two inline TTL-driven electronic switches (Ocean Optics, Inc., Dunedin, FL, USA) [46]; (5) a bare optic fiber probe (field of view (FOV) of 20°) and a fiber optic probe (FOV of 180°) connected to the cosine corrector (CC3-3-UV-S, Ocean Optics, Inc., Dunedin, FL, USA); and (6) an automatic radiator to maintain the temperature inside the instrument case [46]. The fiber optic probe with cosine corrector and the bare fiber optic probe are used to collect the downlink solar incidence spectrum and the uplink feature canopy reflection spectrum, respectively, and the collected spectra are sequentially passed through the long fiber and electronic switch connected to the corresponding probes to form two spectral channels, which reach the bifurcated end of the Y-shaped bifurcated fiber and finally arrive inside the QE65 Pro spectrometer.

The SIF observation system uses a "sandwich" mode to collect spectral data [47]. A dataset consists of three spectral acquisitions, the downlinked solar incidence spectrum, the uplinked feature canopy reflection spectrum, and the downwelling solar incidence spectrum, which are acquired by controlling the alternate opening and closing of two electronic switches [46]. Since the mismatch of time between measurements of downwelling and upwelling introduces errors due to weather variations, the downwelling solar incidence spectrum is represented by the average of the two measured downwelling solar incidence spectra. Before acquisition of each spectrum, the spectrometer optimally determines the integration time based on the received spectral signal and records the dark current [46]. Under normal conditions, a complete set of data acquisition takes about 15 seconds during midday, and about two minutes during sunrise and sunset.

2.3. Meteorological Variables and Flux Observations

An automatic weather station (AWS) was utilized to observe meteorological variables, which was mounted on the AR site flux tower platform and could observe several meteorological variables including air temperature (Ta), barometric pressure (p), relative humidity (Rh), precipitation, wind speed/direction, and photosynthetically active radiation (PAR); measurements were recorded every 10 min [48]. Half-hourly averaged meteorological data were obtained by averaging multiple 10-min data over a half-hour period, and daily averaged meteorological data were obtained by re-averaging daily half-hourly averaged data.

Alpine meadow and atmospheric exchange of energy, carbon dioxide, and water were measured by an eddy covariance (EC) system, which was also mounted on the tower-based platform around three meters from the ground [48]. The EC system includes a three-dimensional acoustic anemometer (CSAT3, Campbell Scientific Inc., Logan, UT, USA) and an open path gas analyzer (Li-7500, Li-Cor, Lincoln, NE, USA) [48,49]. The data sampling frequency is 10 Hz. We filled in the gaps in the data with the online resource tool (http://www.bgc-jena.mpg.de/~MDIwork/eddyproc/ (accessed on 24 September 2021)) supplied by the Max Planck Institute for Biogeochemistry (MPI-BGC). Based on data for the measured CO_2 net ecosystem exchange flux (NEE) and meteorological variables, a division of inter-day NEE into GPP and ecosystem respiration was performed using the inter-day division method proposed by Lasslop et al. [50]. The final separation was obtained for half-hourly GPP data. The daily averaged GPP data were obtained by re-averaging daily half-hourly averaged data.

2.4. Canopy SIF Retrieval

Canopy SIF (SIF$_{Red}$, SIF$_{Far-red}$) for red and far-red bands were retrieved with spectral fitting method (SFM). The prerequisite assumption for extracting SIF from the reflected radiance spectrum of surface vegetation is that reflectance and fluorescence emission obey Lambert's cosine law, whereby the upwelling radiance of vegetation is coupled by two components: the solar flux reflected, and the fluorescence emitted [51,52]. SFM supposes that reflectance spectra and fluorescence spectra in chosen spectral intervals are functions of wavelengths that can be described by mathematical functions rather than that they are spectrally constant [52]. Here, the reflectance and fluorescence spectra were fitted separately with quadratic functions:

$$L(\lambda) = \frac{r(\lambda)E(\lambda)}{\pi} + F(\lambda) = \frac{(a\lambda^2 + b\lambda + c)E(\lambda)}{\pi} + \left(m\lambda^2 + n\lambda + p\right) \tag{1}$$

where λ is wavelength, $L(\lambda)$ is the radiance upwelling from vegetation, $r(\lambda)$ is the reflectance (without the emission component), $E(\lambda)$ is the incoming total solar irradiance to the target, $F(\lambda)$ is the solar-induced fluorescence, and a, b, c, m, n, and p are the spectral fitting coefficients, respectively.

2.5. Statistical Analysis and Model Fitted

To reduce the confounding due to backgrounds, such as soil, and the effect of scattered light ratios from direct light, only spectral data with NDVI > 0.5 and SZA < 80° were used.

$$NDVI = \frac{R_{NIR} - R_{Red}}{R_{NIR} + R_{Red}} \tag{2}$$

where R_{NIR} and R_{Red} represent the reflectance at near-infrared (NIR) and red bands. Here, the average reflectance of 780–800 nm and 681–685 nm was used to stand for the NIR and red band reflectance, respectively.

The existence of coupling between SIF and GPP has been illustrated in a variety of studies on various platforms, scales, and ecosystems, but whether the link between SIF and GPP is linear or nonlinear remains inconclusive [28,53]. Previous studies indicated that the SIF-GPP relationship is linear [26,30], but mounting studies have shown that the SIF-GPP relationship tends to be more nonlinear as the data temporal resolution improves [54–56]. Because of this, two fitted models, linear and nonlinear, were used to depict the SIF-GPP relationship for the 30-min averaged data, while for the daily averaged data, only the linear fitted model was used.

$$GPP_{Linear} = k \times SIF \tag{3}$$

$$GPP_{Nonlinear} = \frac{p_1 \times SIF + p_2}{SIF + p_3} \tag{4}$$

where GPP_{Linear} stands for the fitted results of SIF with the linear model, $GPP_{Nonlinear}$ stands for the fitted results of SIF with the nonlinear model, and k, p_1, p_2, and p_3 stand for the fitted parameters of the models.

The merits of the fitted models were then evaluated using R^2 and the root mean square error (RMSE) for a comprehensive evaluation.

3. Results

3.1. Seasonal Patterns of SIF and GPP and Their Relationship

Due to instrument failures, there were some data gaps for alpine meadow spectral and flux data in both the 2019 and 2020 growing seasons, but the available data could cover most growing stages of alpine meadow. Figure 2 illustrates the seasonal variations of SIF$_{Red}$, SIF$_{Far-red}$, GPP, and NDVI. At the seasonal scale, they show consistent and obvious "single-peaked" seasonal patterns. NDVI reaches its maximum value for the whole growing season at about 205–220 days of day of year (DOY), and the corresponding SIF$_{Red}$, SIF$_{Far-red}$,

and GPP also reach their maximum values during the same period. There is relatively small variation in the seasonality of photosynthetically active radiation (PAR), with generally high PAR values over the entire growing season.
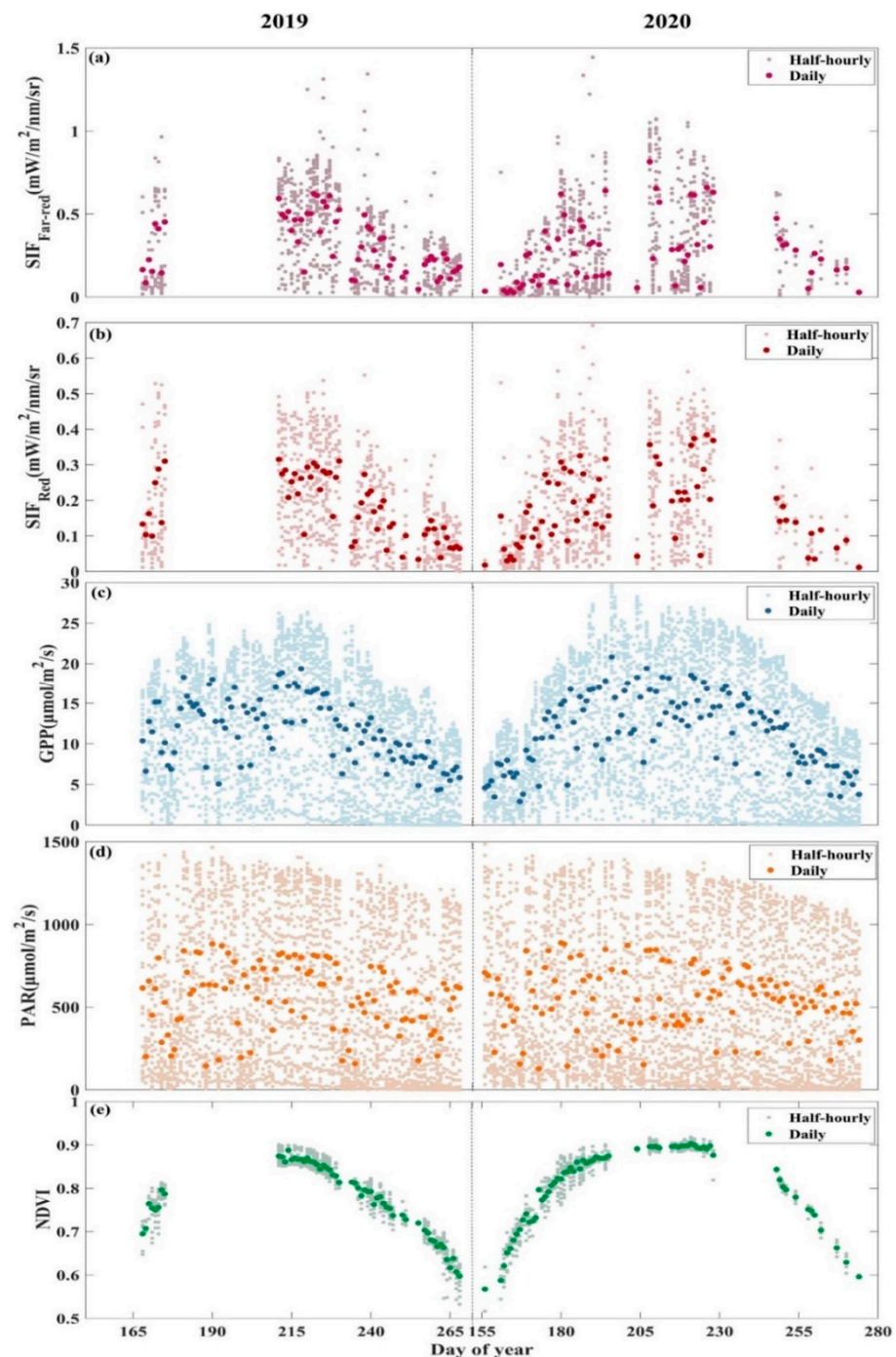

Figure 2. Seasonal patterns of (**a**) the canopy solar-induced chlorophyll fluorescence at the far-red band ($SIF_{Far-red}$), (**b**) the canopy solar-induced chlorophyll fluorescence at the red band (SIF_{Red}), (**c**) gross primary productivity (GPP), (**d**) photosynthetically active radiation (PAR), (**e**) normalized difference vegetation index (NDVI) at AR site in the growing seasons in 2019 (**left**) and 2020 (**right**). The dark large dots represent daily averaged data, and the light small dots represent half-hourly averaged data.

The relationships between SIF_{Red} and $SIF_{Far-red}$ with GPP in alpine meadows were analyzed with half-hourly and daily averaged datasets. Both a linear function model

($y = kx$), with the intercept of the linear function set to zero, and a nonlinear function model ($y = (p_1 x + p_2)/(x + p_3)$) were adopted to fit SIF and GPP relationship (Table 1). The differences in R^2 between the nonlinear and linear fitted function models for the SIF_{Red}-GPP relationship are small with regard to both half-hourly and daily averaged data and are larger for the $SIF_{Far-red}$-GPP relationship, especially concerning the half-hourly averaged data, where the R^2 of the fitted results of the nonlinear function model is 12.86% higher than that of the linear function model. The difference in RMSE between the nonlinear and linear fitted function models for both SIF_{Red}-GPP and $SIF_{Far-red}$-GPP is obvious; for the half-hourly data, the RMSE of the linear fitted results for SIF_{Red}-GPP and $SIF_{Far-red}$-GPP are 31.49% and 59.44% higher than the corresponding nonlinear fitted results, respectively, and for the daily averaged data, 24.89% and 64.93% higher, respectively. Although for both SIF_{Red}-GPP and $SIF_{Far-red}$-GPP, the RMSE of the linear fitted results are higher than the nonlinear fitted results for both the half-hourly and daily averaged data, considering the R^2 of the fitted results and the scatter plot distribution of the data together (Figure 3), the SIF_{Red}-GPP relationship tends to be more linear than the $SIF_{Far-red}$-GPP relationship. The R^2 of the linear fitted SIF_{Red}-GPP relationship and that of the nonlinear fitted $SIF_{Far-red}$-GPP relationship are also close. These results indicate that the performance of SIF_{Red} and $SIF_{Far-red}$ were comparable for monitoring GPP in an alpine meadow.

Table 1. Statistical results of linear and nonlinear fitting for SIF_{Red} and $SIF_{Far-red}$ with GPP.

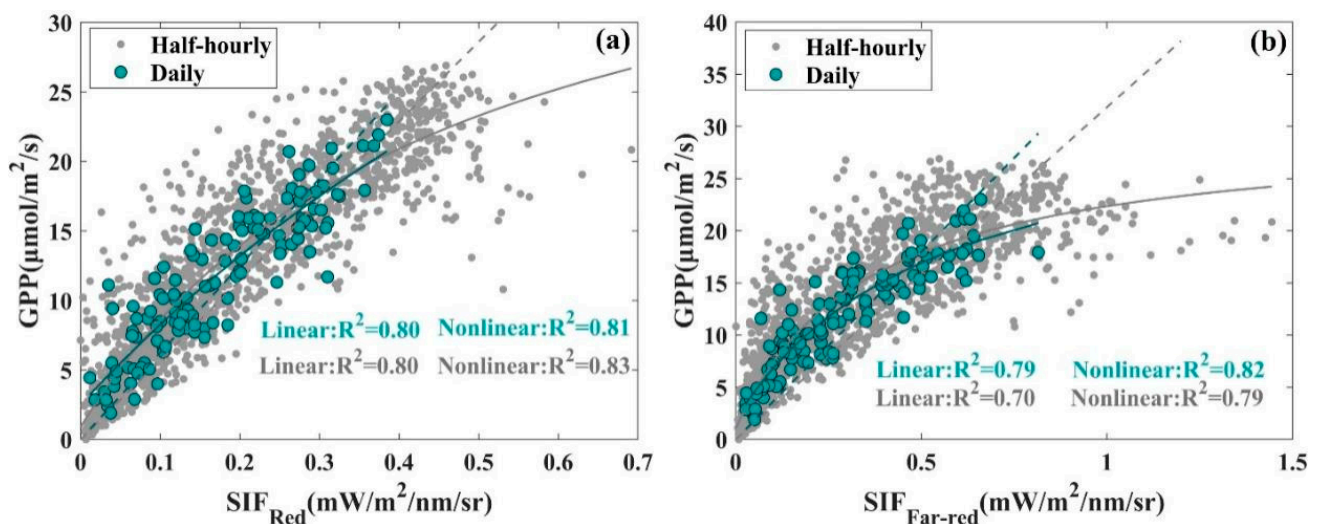| Temporal Resolution		Half-Hourly		Daily	
Mathematical Function Model		**Linear**	**Nonlinear**	**Linear**	**Nonlinear**
SIF_{Red}	Formula	$y = 57.23x$	$y = \frac{43.69x+0.40}{x+0.45}$	$y = 62.52x$	$y = \frac{79.24x+3.09}{x+1.23}$
	R^2	0.80	0.83	0.80	0.81
	RMSE	3.80	2.89	2.76	2.21
$SIF_{Far-red}$	Formula	$y = 31.84x$	$y = \frac{29.99x+0.37}{x+0.36}$	$y = 35.97x$	$y = \frac{33.46x+1.05}{x+0.55}$
	R^2	0.70	0.79	0.79	0.82
	RMSE	5.15	3.23	3.48	2.11

Figure 3. The relationship between SIF_{Red} (**a**), $SIF_{Far-red}$ (**b**), and GPP at the seasonal scale at the AR site, large green dots represent daily averaged data, small gray dots represent half-hourly averaged data, the dashed lines represent linear fit lines, the solid lines represent non-linear fit lines, and the green and gray lines represent the daily averaged data fit lines and the half-hourly averaged data fit lines of SIF and GPP, respectively.

3.2. Response of SIF and GPP to Environmental Factors

The impact of environmental factors upon the SIF-to-GPP ratio was also analyzed. As shown in Figure 4, with increasing PAR values, SIF_{Red}/GPP values show a very slight increasing trend, while $SIF_{Far-red}/GPP$ values show an obvious increasing trend, with obvious increases when PAR is higher than 400–600 µmol/m^2/s. SIF_{Red}/GPP values remain almost constant across different changes in Ta without obvious variations, while those of $SIF_{Far-red}/GPP$ show an increasing trend, especially when the temperature increases to 15 °C, where $SIF_{Far-red}/GPP$ shows a substantial increase. In addition, SIF_{Red}/GPP values did not show obvious variations across different changes in VPD, while $SIF_{Far-red}/GPP$ values showed an obvious increasing trend with increases in VPD. In general, for the same value of a given environmental factor, the SIF_{Red}/GPP values tended to be concentrated and have smaller variance, while those of $SIF_{Far-red}/GPP$ were dispersed and had larger variance. When there were changes in the value of the given environmental factor, the SIF_{Red}/GPP values tended to vary less in response and those of $SIF_{Far-red}/GPP$ vary more. This indicates that SIF_{Red} and GPP tended to have a more consistent response to changes in environmental factors than $SIF_{Far-red}$ and GPP.

At the diurnal scale, first, observations from two days with similar PAR but different Ta and VPD were selected to analyze the impacts of environmental factors on SIF-GPP relationship at red and far-red band for alpine meadow. The diurnal variations and values of PAR are similar for DOY220 and DOY227 as shown in Figure 5, while changes in Ta and VPD are obvious, i.e., the values of Ta and VPD for DOY220 are lower than those for DOY227. Due to the decrease in Ta and VPD, the R^2 of the linear fitted with zero intercept of both SIF_{Red}-GPP and $SIF_{Far-red}$-GPP underwent serious decrease and the RMSE underwent dramatic increase in DOY220, with 29.63% and 40% decrease in R^2 and about one and three times increase in RMSE for SIF_{Red}-GPP and $SIF_{Far-red}$-GPP, respectively. Comparing the SIF-GPP relationship for these two days, we found that the slope of the linear fitted with zero intercept between $SIF_{Far-red}$ and GPP decreased obviously when there was an obvious decrease in Ta and VPD values, i.e., of 24.35%, while the slope of the linear fit between SIF_{Red} and GPP did not show any obvious differences.

Furthermore, we selected a typical sunny day and a cloudy day, between which there were obvious differences in the daily changes of PAR, Ta, and VPD. We analyzed the variations in the relationship of SIF_{Red} and $SIF_{Far-red}$ with GPP separately for these two days. From the sunny day to the cloudy day, the R^2 of the linear fitted with zero intercept for SIF_{Red}-GPP increased by 7.69% and the RMSE decreased appreciably, by 64.78%, with the scattered distribution of the data on the cloudy day being closer to the fitted line compared to the sunny day, while the R^2 of $SIF_{Far-red}$-GPP decreased by 5.75% and the RMSE increased by 4.6%. As shown in Figure 6, the slopes of the linear fitted with zero intercept between $SIF_{Far-red}$ and SIF_{Red} with GPP are both obviously steeper under cloudy weather than those under sunny weather, though the degree of changes in the slopes differ. For SIF_{Red} and GPP, the slope of the linear fitted is approximately 1.6 times higher under cloudy weather than those under sunny weather, while for $SIF_{Far-red}$ and GPP, it is approximately 2.5 times higher.
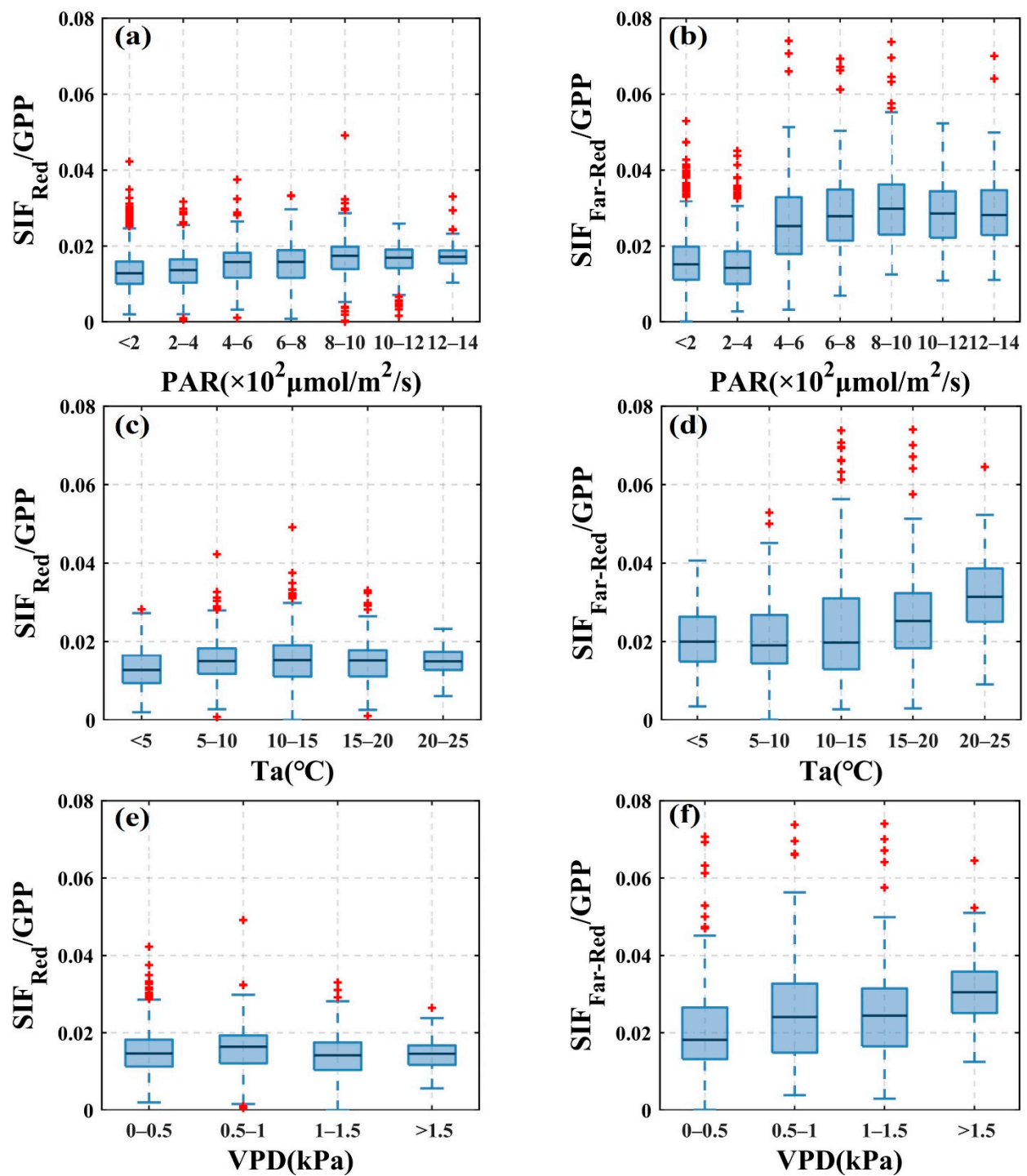
Figure 4. Boxplots show the variation of values of SIF_{Red}/GPP and $SIF_{Far-red}$/GPP at different levels of environmental factors including (**a**,**b**) photosynthetically active radiation (PAR), (**c**,**d**) air temperature (Ta), and (**e**,**f**) vapor pressure deficit (VPD) at AR site during the 2019 (**left**) and 2020 (**right**) growing seasons with half-hourly averaged data. Red plus signs in the figure represent outliers.
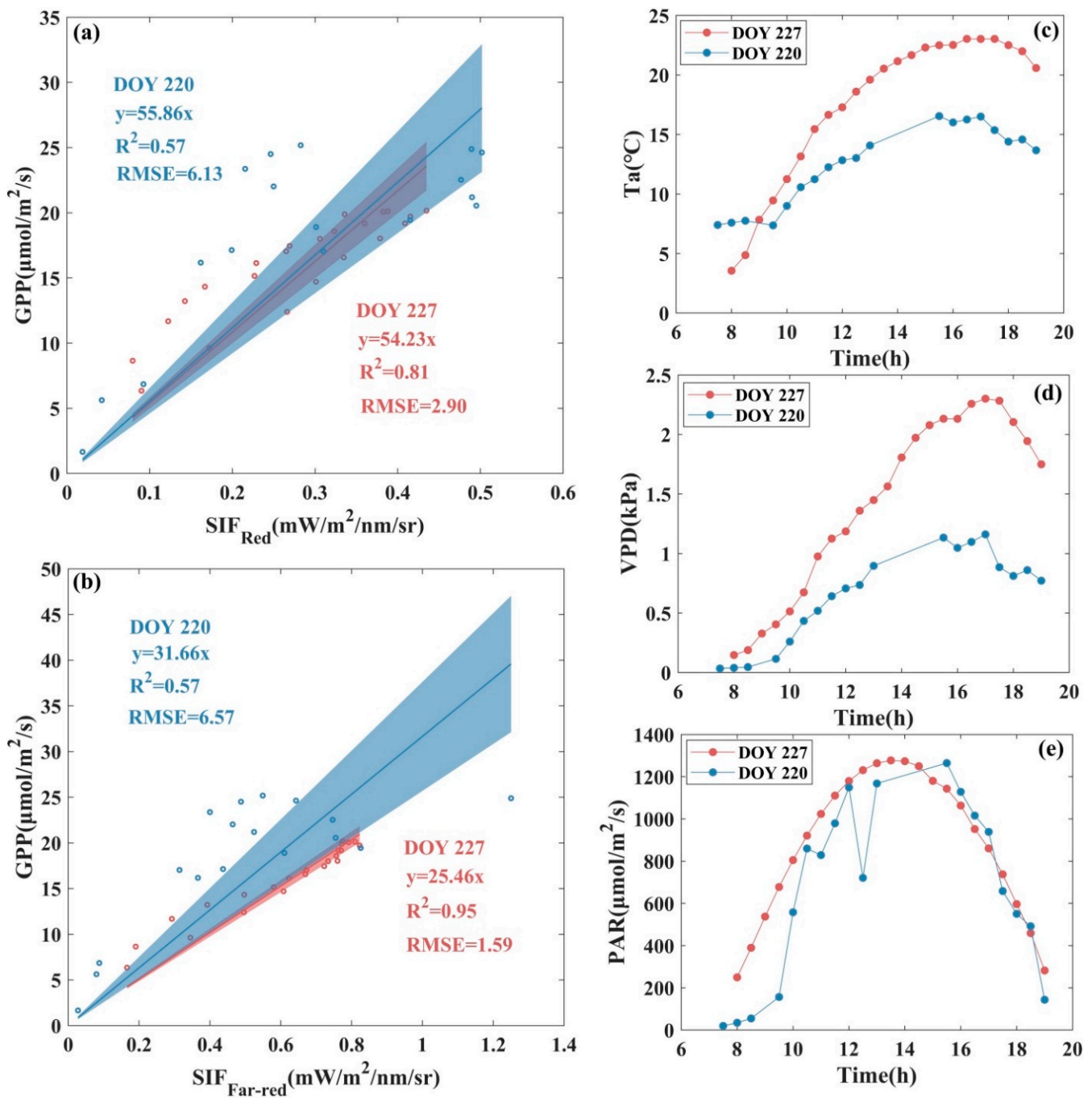
Figure 5. Scatter plot of the fitted relationship between (**a**) SIF$_{Red}$, (**b**) SIF$_{Far-red}$, and GPP at the diurnal scale and daily variations of (**c**) air temperature (Ta), (**d**) vapor pressure deficit (VPD), and (**e**) photosynthetically active radiation (PAR) for DOY220 and DOY227 in 2020 at AR site. The scatter points represent half-hourly averaged data, the solid line represents the fitted line of the SIF-GPP relationship, and the shaded area indicates the 95% confidence level of the prediction, where red represents DOY227, and blue represents DOY220.
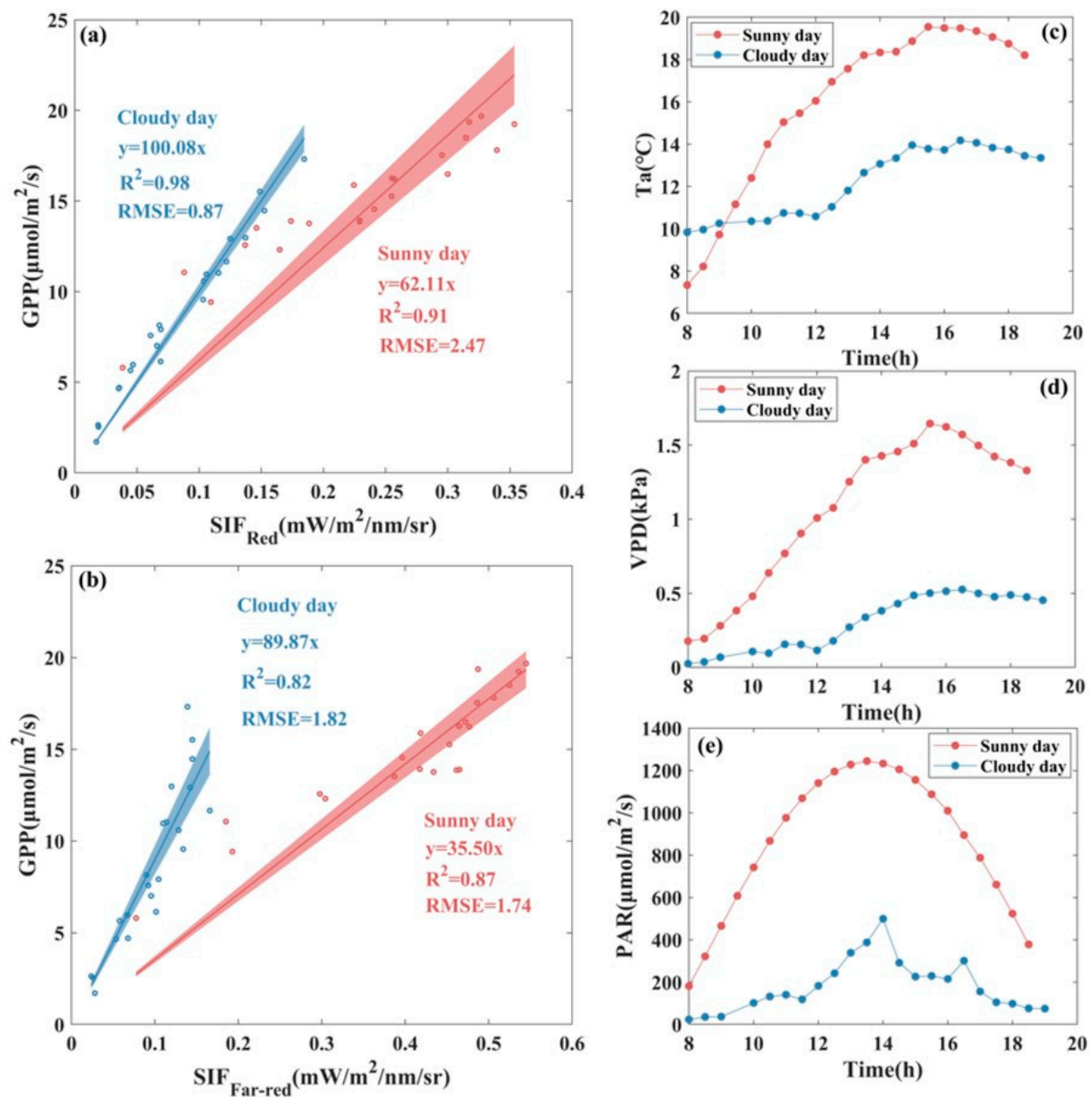
Figure 6. Scatter plot of the fitted relationship between (**a**) SIF$_{Red}$, (**b**) SIF$_{Far-red}$, and GPP at the diurnal scale and daily variations of (**c**) air temperature (Ta), (**d**) vapor pressure deficit (VPD), and (**e**) photosynthetically active radiation (PAR) for a typical sunny day and cloudy day at AR site. The scatter points represent half-hourly averaged data, the solid line represents the fitted line of the SIF-GPP relationship, and the shaded area indicates the 95% confidence level of the prediction, where red represents sunny day and blue represents cloudy day.

4. Discussion

4.1. Reasons Why Red SIF Shows More Potential Than Far-Red SIF for Monitoring GPP in an Alpine Meadow Ecosystem

At present, researchers have not reached a definite conclusion as to which has greater potential for monitoring GPP in various ecosystems, red SIF or far-red SIF. Most previous studies at the canopy level have shown that the potential of red SIF for monitoring GPP was limited by strong reabsorption effects within the canopy and relatively low retrieval accuracy [9,14,27]. However, the results in this study show that red SIF had even more

potential than far-red SIF in monitoring GPP in an alpine meadow ecosystem. Here are several possible main reasons for this result.

First of all, we obtained a relatively high precision SIF inversion result for the red and far-red bands. The specifications of the instruments used to measure the spectra and the spectral properties of the irradiance and the reflectance spectra at the absorption bands affect the accuracy of SIF retrieval [57]. In this study, measurements of the continuous spectrum were performed using the SIFSpec system, the core of which is a customized Ocean Optics QE65 Pro spectrometer having high signal-to-noise ratio (>1000) and high spectral resolution (~0.34 nm), ensuring the quality and accuracy of the collected spectral data. Meanwhile, the SFM algorithm was used for the inversion of canopy SIF. The SFM algorithm uses mathematical functions to, first, model the reflectance and fluorescence spectral curves and then invert the chlorophyll fluorescence intensity. In a narrow spectral range, relatively simple fluorescence and reflectance spectral curves can be fitted relatively accurately using polynomial functions. In this study, a quadratic polynomial function was used to fit the spectral curves in both absorption bands of O_2-A and O_2-B, therefore, high-precision canopy SIF inversion results were obtained for both bands.

For the second, the theoretical basis for red SIF to be sensitive to physiological changes in vegetation. SIF contains APAR information, and it also contains, to some extent, energy distribution information at the photosystem level [11,17,20]. There are two photosynthetic reaction systems in the mechanism of photosynthesis in higher plants, photosystem I (PS I) and photosystem II (PS II) [58,59]. Variable plant fluorescence is observed for PS II due to changes in plant physiological conditions, but this variable fluorescence is not observed for PS I [11,60,61]. SIF emission in the far-red band is performed by PS I and PS II, while SIF emission in the red band is mainly performed by PS II [11,62]. Therefore, theoretically, the SIF in the red contributed mostly by PS II shows greater responsiveness to changes in the physiological condition of vegetation [11]. Previously, several studies have reported the potential of red SIF in monitoring GPP. For example, Liu et al. [38] showed that after downscaling the red SIF of the maize canopy to the photosystem level, an obvious improvement in the red SIF and GPP correlation was achieved. Their findings also showed that at the photosystem level, red SIF monitored GPP equally well or even better than far-red SIF, which indicated that after removing the effect of canopy reabsorption, red SIF could provide more effective information on plant photosynthesis and physiology and, thus, red SIF was more related to GPP than far-red SIF. Joiner et al. [58] also observed that fluorescence in the red band was more sensitive to GPP than fluorescence in the far-red band under drought stress. Hence, from a plant physiological perspective, the strong correlation between PSII and SIF_{Red} may be one of the reasons for the performance of SIF_{Red} being better than that of $SIF_{Far-red}$ in monitoring GPP in this alpine meadow ecosystem.

Last but not least, the red SIF showed a linear correlation with GPP in this alpine meadow ecosystem. That linear relationship between red SIF and GPP is more advantageous for GPP tracking than the nonlinear relationship between far-red SIF and GPP. Alpine meadow ecosystems are dominated by grasses with relatively low leaf area index values, and the resorption effect within the canopy is likely to be relatively small. However, during a period of vigorous vegetation growth, the SIF in the red band is probably inevitably affected by the reabsorption effect. For example, following the downscaling of grass and wheat canopy SIF to the photosystem level using the random forest method, Liu et al. [63] found that the correlation between red SIF at the photosystem level and chlorophyll absorption of photosynthetically active radiation was remarkably enhanced compared to red SIF at the canopy level. This also implied that the red SIF is mainly influenced by the internal reabsorption effect of leaves. Therefore, it is reasonable to speculate that the red SIF observed in the alpine meadow canopy was saturated due to the reabsorption effect. Moreover, many studies have confirmed that the relationship between GPP and absorption of photosynthetically active radiation is nonlinear and that GPP will saturate when the APAR reaches a certain level [40,56]. Therefore, the saturation phenomenon that occurred for both GPP and SIF_{Red} resulted in a linear relationship between the two. While

the far-red SIF is mainly affected by canopy scattering, and the effect of reabsorption on it can be basically ignored [43,63], thus the far-red SIF does not exist saturation phenomenon. When PAR reached a certain level, GPP no longer increased, while far-red SIF was still increasing, thus far-red SIF showed a nonlinear correlation with GPP in this alpine meadow ecosystem. As the time resolution of the data was reduced from half-hourly average to daily average, there was smoothing of the data noise and variance, which led to a reduction in the difference between the results of fitted $SIF_{Far-red}$ to GPP with nonlinear and linear functions under the daily averaged data. Nevertheless, from the trend of data distribution, whether half-hourly or daily averaged data, GPP showed a more linear relationship with red SIF than with far-red SIF.

4.2. Differences in the Response of SIF_{Red}/GPP and $SIF_{Far-red}$/GPP to Changes in Environmental Factors

How well synchronized the SIF and GPP are in response to environmental changes affects the accuracy of SIF estimation of GPP. Alpine meadow ecosystems are sensitive to environmental changes [3,5–7]. For the alpine meadow ecosystem at the AR site, the average annual Ta is low. Even in summer, frosts may still occur in the early morning [64]. The AR station is at high altitude and has high levels of harmful ultraviolet-B radiation, it also has sufficient radiation and sufficient hours of sunshine to allow plants to perform normal photosynthesis to maintain their organic growth. VPD also has a range of fluctuations in this alpine meadow ecosystem. The level of VPD has a direct effect on the stomatal conductance of plant leaves. Excessive VPD leads to decrease in stomatal conductance to prevent excessive water loss in plants, though this inevitably reduces the CO_2 uptake of photosynthesis and affects the photosynthetic process.

In this research, the ratio of SIF_{Red}/GPP was found more stable than $SIF_{Far-red}$/GPP as environmental factors varied at the seasonal scale. We investigated the relationship between SIF_{Red}-GPP and $SIF_{Far-red}$-GPP with seasonal changes in PAR, Ta, and VPD at seasonal scales using the ratio of SIF to GPP. As Ta, VPD levels varied along the *x*-axis, SIF_{Red}/GPP was able to remain relatively stable, and the boxes at different levels in Figure 4c,e were roughly on the same level, indicating that the sensitivity of SIF_{Red} and GPP to changes in Ta and VPD were similar. Therefore, the magnitude of SIF_{Red}/GPP values did not change obviously on the seasonal scale. Compared to the stability of SIF_{Red}/GPP, the value of $SIF_{Far-red}$/GPP showed a more obvious fluctuation with the variation of Ta and VPD and showed an increasing trend. Both Ta and VPD can cause physiological activity alterations in vegetation as Ta variations cause changes in photosynthetic enzyme activity, while VPD variations change the degree of opening of vegetation stomatal conductance. Red SIF is more closely correlated with changes in vegetation physiological activity and may provide more timely feedback than far-red SIF on physiological changes such as photosynthetic carbon assimilation due to environmental changes [11], and this may explain why SIF_{Red}/GPP was more stable than $SIF_{Far-red}$/GPP. As shown in Figure 4, when PAR levels varied along the *x*-axis, SIF_{Red}/GPP also showed slight fluctuations after PAR reached a certain level, but obviously not as much as $SIF_{Far-red}$/GPP. As discussed in Section 4.1, both the red SIF and GPP were probably saturated, but likely the degree of saturation was different for both, resulting in slight fluctuations in SIF_{Red}/GPP. While saturation occurred in GPP, the far-red SIF value was still increasing, thus leading to large fluctuations with an increasing trend in the value of $SIF_{Far-red}$/GPP. These results are consistent with the conclusions obtained in Figure 2.

PAR dominated the variation in the slope of the linear fitted line with zero intercept for SIF-GPP at the diurnal scale among the three environmental factors investigated in this research. At the diurnal scale, when PAR experienced an obvious drop, the slope of the linear fitted line between SIF and GPP changed by 107.14% on average, while when Ta and VPD had an obvious drop, the slope of the linear fitted line between SIF and GPP changed by only 13.68% on average. Thus, combining Figures 5 and 6, it is evident that the slope variation of the linear fitted line of SIF versus GPP depended more on PAR than on Ta and

VPD. The slope of the linear fitted line between SIF_{Red} and GPP varied obviously less than that between $SIF_{Far-red}$ and GPP. This also indicated that the red SIF was more similar than the far-red SIF in response to environmental changes with GPP. Both red SIF and far-red SIF correlated stronger with GPP on the cloudy day than on the sunny day. This result is consistent with previous results in crops [31] and forests ecosystems [35]. On cloudy days, the proportion of scattered light increases, which penetrates into the lower leaves of the plant and the light-use efficiency of the plants gets improved [16,23], leading to a larger slope of the linear fitted of SIF to GPP.

Against the background of global climate change, alpine meadow ecosystems will face a very uncertain growth environment, in which changes in meteorological environmental factors will be unpredictable. The estimation of GPP in alpine meadow ecosystems urgently needs a stable indicator, and the results of this paper exactly demonstrated the potential of red SIF to track GPP in alpine meadow ecosystems when environmental changes occur.

4.3. Limitations and Uncertainties

Benefiting from the long-term and continuous observation capability of both the EC system and the Tower Platform Automated spectral observation system, we were able to explore the SIF-GPP relationship in alpine meadow ecosystems at the seasonal and daily scale as well as the response of their relationship to changes in environmental factor levels. However, several limitations and uncertainties still exist here. Firstly, there is a problem of footprint matching and spatial representativeness [65,66]. The spectral and flux observation are often prone to the problem of footprint mismatch [67]. At this research site, the EC system and the tower-based automatic spectral observation system were positioned on the same tower, and the spectral observation coverage was included in the flux observation coverage. The underlying surface of the AR station is flat and homogeneous, so the footprint mismatch problem was expected to have little impact on this study. However, given that only one alpine meadow ecosystem observation station at the AR site was involved, whether the conclusions obtained in this study are applicable to all alpine meadow ecosystems needs further study. Secondly, there is the problem of observation geometry. The probe of our tower-based platform automatic spectroscopic observation system was placed heading southwest. We have removed the observation data with solar azimuth angle greater than $80°$ in order to ensure the data quality. However, the change of solar azimuth angle through the day still lead to the appearance of shadows in the observation field of view, which would certainly introduce errors to the inversion of canopy SIF. The effect of solar observation geometry should be considered in future studies. Thirdly, we merely conducted observational studies on canopy-scale SIF and GPP in alpine meadows at AR stations, without involving the measurement of canopy structural and physiological parameters in alpine meadows, which should be included in future studies to enable us to analyze the relationship between SIF and GPP more comprehensively from a physiological perspective. Finally, recent studies have highlighted the excellent performance of NIR_V in tracking GPP [68,69], but NIR_V reflects more information on vegetation canopy structure [70], while SIF is directly related to vegetation photosynthetic processes [16]. In the future study, we will investigate the superior and inferior performance of NIRV and SIF in tracking GPP in alpine meadow ecosystems.

5. Conclusions

In this study, we acquired canopy spectral data, meteorological data, and flux data in 2019 and 2020 alpine meadow growing seasons using a continuous tower-based automated SIF and flux observation system to investigate SIF_{Red} and $SIF_{Far-red}$ in terms of their performance in monitoring GPP in an alpine meadow ecosystem. Our results show that canopy SIF can effectively monitor GPP in alpine meadow ecosystem at both the seasonal and diurnal scales. In particular, SIF_{Red} presented a linear relationship with GPP, while $SIF_{Far-red}$ presented a nonlinear relationship with GPP, and the performance of SIF_{Red} for monitoring GPP was comparable to that of $SIF_{Far-red}$. PAR, VPD, and Ta affected $SIF_{Far-red}/GPP$ more

than SIF_{Red}/GPP at the seasonal scale. Red SIF was more similar with GPP than far-red SIF in response to seasonal changes in environmental factors. PAR dominated the influence on the diurnal-scale variation of the SIF-GPP relationship among the three environmental impact factors considered in this research. Altogether, the red band SIF-GPP relationship was more robust when the environmental factors changed compared to the far-red band. The results of this study highlight the potential of utilizing red SIF for GPP monitoring in alpine meadow ecosystems.

References

1. Gu, S.; Tang, Y.H.; Du, M.Y.; Kato, T.; Li, Y.N.; Cui, X.Y.; Zhao, X.Q. Short-term variation of CO_2 flux in relation to environmental controls in an alpine meadow on the Qinghai-Tibetan Plateau. *J. Geophys. Res. Atmos.* **2003**, *108*. [CrossRef]
2. Kato, T.; Tang, Y.H.; Gu, S.; Hirota, M.; Du, M.Y.; Li, Y.N.; Zhao, X.Q. Temperature and biomass influences on interannual changes in CO_2 exchange in an alpine meadow on the Qinghai-Tibetan Plateau. *Glob. Chang. Biol.* **2006**, *12*, 1285–1298. [CrossRef]
3. Wang, Y.Y.; Xiao, J.F.; Ma, Y.M.; Luo, Y.Q.; Hu, Z.Y.; Li, F.; Li, Y.N.; Gu, L.L.; Li, Z.G.; Yuan, L. Carbon fluxes and environmental controls across different alpine grassland types on the Tibetan Plateau. *Agric. For. Meteorol.* **2021**, *311*, 108694. [CrossRef]
4. Saito, M.; Kato, T.; Tang, Y. Temperature controls ecosystem CO_2 exchange of an alpine meadow on the northeastern Tibetan Plateau. *Glob. Chang. Biol.* **2009**, *15*, 221–228. [CrossRef]
5. Wang, Y.Y.; Ma, Y.M.; Li, H.X.; Yuan, L. Carbon and water fluxes and their coupling in an alpine meadow ecosystem on the northeastern Tibetan Plateau. *Theor. Appl. Climatol.* **2020**, *142*, 1–18. [CrossRef]
6. Wang, Y.X.; Sun, Y.; Chang, S.H.; Wang, Z.F.; Fu, H.; Zhang, W.G.; Hou, F.J. Restoration Practices Affect Alpine Meadow Ecosystem Coupling and Functions. *Rangel. Ecol. Manag.* **2020**, *73*, 441–451. [CrossRef]
7. Zhang, T.; Zhang, Y.J.; Xu, M.J.; Zhu, J.; Chen, N.; Jiang, Y.B.; Huang, K.; Zu, J.X.; Liu, Y.J.; Yu, G.R. Water availability is more important than temperature in driving the carbon fluxes of an alpine meadow on the Tibetan Plateau. *Agric. For. Meteorol.* **2018**, *256*, 22–31. [CrossRef]
8. Baldocchi, D.; Chu, H.; Reichstein, M. Inter-annual variability of net and gross ecosystem carbon fluxes: A review. *Agric. For. Meteorol.* **2018**, *249*, 520–533. [CrossRef]
9. Liu, X.J.; Liu, Z.Q.; Liu, L.Y.; Lu, X.L.; Chen, J.D.; Du, S.S.; Zou, C. Modelling the influence of incident radiation on the SIF-based GPP estimation for maize. *Agric. For. Meteorol.* **2021**, *307*, 108522. [CrossRef]
10. Wang, X.F.; Ma, M.G.; Huang, G.H.; Veroustraete, F.; Zhang, Z.H.; Song, Y.; Tan, J.L. Vegetation primary production estimation at maize and alpine meadow over the Heihe River Basin, China. *Int. J. Appl. Earth Obs. Geoinf.* **2012**, *17*, 94–101. [CrossRef]
11. Guanter, L.; Zhang, Y.G.; Jung, M.; Joiner, J.; Voigt, M.; Berry, J.A.; Frankenberg, C.; Huete, A.R.; Zarco-Tejada, P.; Lee, J.E.; et al. Global and time-resolved monitoring of crop photosynthesis with chlorophyll fluorescence. *Proc. Natl. Acad. Sci. USA* **2014**, *111*, E1327–E1333. [CrossRef] [PubMed]
12. Hilker, T.; Coops, N.C.; Wulder, M.A.; Black, T.A.; Guy, R.D. The use of remote sensing in light use efficiency based models of gross primary production: A review of current status and future requirements. *Sci. Total Environ.* **2008**, *404*, 411–423. [CrossRef] [PubMed]
13. Li, X.; Xiao, J.F.; He, B.B.; Altaf Arain, M.; Beringer, J.; Desai, A.R.; Emmel, C.; Hollinger, D.Y.; Krasnova, A.; Mammarella, I.; et al. Solar-induced chlorophyll fluorescence is strongly correlated with terrestrial photosynthesis for a wide variety of biomes: First global analysis based on OCO-2 and flux tower observations. *Glob. Chang. Biol.* **2018**, *24*, 3990–4008. [CrossRef] [PubMed]
14. Goulas, Y.; Fournier, A.; Daumard, F.; Champagne, S.; Ounis, A.; Marloie, O.; Moya, I. Gross Primary Production of a Wheat Canopy Relates Stronger to Far Red Than to Red Solar-Induced Chlorophyll Fluorescence. *Remote Sens.* **2017**, *9*, 97. [CrossRef]
15. Baker, N.R. Chlorophyll fluorescence: A probe of photosynthesis in vivo. *Annu. Rev. Plant Biol.* **2008**, *59*, 89–113. [CrossRef]

16. Porcar-Castell, A.; Tyystjarvi, E.; Atherton, J.; van der Tol, C.; Flexas, J.; Pfundel, E.E.; Moreno, J.; Frankenberg, C.; Berry, J.A. Linking chlorophyll a fluorescence to photosynthesis for remote sensing applications: Mechanisms and challenges. *J. Exp. Bot.* **2014**, *65*, 4065–4095. [CrossRef]

17. Sun, Y.; Frankenberg, C.; Wood, J.D.; Schimel, D.S.; Jung, M.; Guanter, L.; Drewry, D.T.; Verma, M.; Porcar-Castell, A.; Griffis, T.J.; et al. OCO-2 advances photosynthesis observation from space via solar-induced chlorophyll fluorescence. *Science* **2017**, *358*, eaam5747. [CrossRef]

18. Krause, G.H.; Weis, E. Chlorophyll fluorescence and photosynthesis the basics. *Annu. Rev. Plant Physiol.* **1991**, *42*, 313–349. [CrossRef]

19. Frankenberg, C.; Fisher, J.B.; Worden, J.; Badgley, G.; Saatchi, S.S.; Lee, J.-E.; Toon, G.C.; Butz, A.; Jung, M.; Kuze, A.; et al. New global observations of the terrestrial carbon cycle from GOSAT: Patterns of plant fluorescence with gross primary productivity. *Geophys. Res. Lett.* **2011**, *38*. [CrossRef]

20. Yang, P.Q.; van der Tol, C.; Verhoef, W.; Damm, A.; Schickling, A.; Kraska, T.; Muller, O.; Rascher, U. Using reflectance to explain vegetation biochemical and structural effects on sun-induced chlorophyll fluorescence. *Remote Sens. Environ.* **2019**, *231*, 110996. [CrossRef]

21. Zhang, Z.; Zhang, Y.; Chen, J.M.; Ju, W.; Migliavacca, M.; El-Madany, T.S. Sensitivity of Estimated Total Canopy SIF Emission to Remotely Sensed LAI and BRDF Products. *J. Remote Sens.* **2021**, *2021*, 9795837. [CrossRef]

22. Miao, G.F.; Guan, K.Y.; Suyker, A.E.; Yang, X.; Arkebauer, T.J.; Walter-Shea, E.A.; Kimm, H.; Hmimina, G.Y.; Gamon, J.A.; Franz, T.E.; et al. Varying Contributions of Drivers to the Relationship Between Canopy Photosynthesis and Far-Red Sun-Induced Fluorescence for Two Maize Sites at Different Temporal Scales. *J. Geophys. Res. Biogeosci.* **2020**, *125*, e2019JG005051. [CrossRef]

23. Chen, J.D.; Liu, X.J.; Du, S.S.; Ma, Y.; Liu, L.Y. Integrating SIF and Clearness Index to Improve Maize GPP Estimation Using Continuous Tower-Based Observations. *Sensors* **2020**, *20*, 2493. [CrossRef]

24. Liu, L.Y.; Guan, L.L.; Liu, X.J. Directly estimating diurnal changes in GPP for C3 and C4 crops using far-red sun-induced chlorophyll fluorescence. *Agric. For. Meteorol.* **2017**, *232*, 1–9. [CrossRef]

25. Yang, K.G.; Ryu, Y.; Dechant, B.; Berry, J.A.; Hwang, Y.; Jiang, C.; Kang, M.; Kim, J.; Kimm, H.; Kornfeld, A.; et al. Sun-induced chlorophyll fluorescence is more strongly related to absorbed light than to photosynthesis at half-hourly resolution in a rice paddy. *Remote Sens. Environ.* **2018**, *216*, 658–673. [CrossRef]

26. Magney, T.S.; Bowling, D.R.; Logan, B.A.; Grossmann, K.; Stutz, J.; Blanken, P.D.; Burns, S.P.; Cheng, R.; Garcia, M.A.; Köhler, P.; et al. Mechanistic evidence for tracking the seasonality of photosynthesis with solar-induced fluorescence. *Proc. Natl. Acad. Sci. USA* **2019**, *116*, 11640–11645. [CrossRef]

27. Liu, Z.Q.; Lu, X.L.; An, S.Q.; Heskel, M.; Yang, H.L.; Tang, J.W. Advantage of multi-band solar-induced chlorophyll fluorescence to derive canopy photosynthesis in a temperate forest. *Agric. For. Meteorol.* **2019**, *279*, 107691. [CrossRef]

28. Yang, H.L.; Yang, X.; Zhang, Y.G.; Heskel, M.A.; Lu, X.L.; Munger, J.W.; Sun, S.C.; Tang, J.W. Chlorophyll fluorescence tracks seasonal variations of photosynthesis from leaf to canopy in a temperate forest. *Glob. Chang. Biol.* **2017**, *23*, 2874–2886. [CrossRef]

29. Huang, Y.; Cheng, Z.; Du, M.H.; Wu, P.F.; Yuan, L.; Tang, J.W. Tidal influence on the relationship between solar-induced chlorophyll fluorescence and canopy photosynthesis in a coastal salt marsh. *Remote Sens. Environ.* **2022**, *270*, 112865. [CrossRef]

30. Miao, G.F.; Guan, K.Y.; Yang, X.; Bernacchi, C.J.; Berry, J.A.; DeLucia, E.H.; Wu, J.; Moore, C.E.; Meacham, K.; Cai, Y.P.; et al. Sun-Induced Chlorophyll Fluorescence, Photosynthesis, and Light Use Efficiency of a Soybean Field from Seasonally Continuous Measurements. *J. Geophys. Res. Biogeosci.* **2018**, *123*, 610–623. [CrossRef]

31. Li, Z.H.; Zhang, Q.; Li, J.; Yang, X.; Wu, Y.F.; Zhang, Z.Y.; Wang, S.H.; Wang, H.Z.; Zhang, Y.G. Solar-induced chlorophyll fluorescence and its link to canopy photosynthesis in maize from continuous ground measurements. *Remote Sens. Environ.* **2020**, *236*, 111420. [CrossRef]

32. Halubok, M.; Yang, Z.L. Estimating Crop and Grass Productivity over the United States Using Satellite Solar-Induced Chlorophyll Fluorescence, Precipitation and Soil Moisture Data. *Remote Sens.* **2020**, *12*, 3434. [CrossRef]

33. Wang, S.H.; Zhang, Y.G.; Ju, W.; Porcar-Castell, A.; Ye, S.S.; Zhang, Z.Y.; Brümmer, C.; Urbaniak, M.; Mammarella, I.; Juszczak, R.; et al. Warmer spring alleviated the impacts of 2018 European summer heatwave and drought on vegetation photosynthesis. *Agric. For. Meteorol.* **2020**, *295*, 108195. [CrossRef]

34. Martini, D.; Sakowska, K.; Wohlfahrt, G.; Pacheco-Labrador, J.; van der Tol, C.; Porcar-Castell, A.; Magney, T.S.; Carrara, A.; Colombo, R.; El-Madanay, T.; et al. Heatwave breaks down the linearity between sun-induced fluorescence and gross primary production. *New Phytol.* **2021**, *233*, 2415–2428. [CrossRef]

35. Cheng, X.F.; Zhou, Y.; Hu, M.J.; Wang, F.; Huang, H.; Zhang, J.S. The Links between Canopy Solar-Induced Chlorophyll Fluorescence and Gross Primary Production Responses to Meteorological Factors in the Growing Season in Deciduous Broadleaf Forest. *Remote Sens.* **2021**, *13*, 2363. [CrossRef]

36. Kim, J.M.; Ryu, Y.; Dechant, B.; Lee, H.; Kim, H.S.; Kornfeld, A.; Berry, J.A. Solar-induced chlorophyll fluorescence is non-linearly related to canopy photosynthesis in a temperate evergreen needleleaf forest during the fall transition. *Remote Sens. Environ.* **2021**, *258*, 112362. [CrossRef]

37. Grossmann, K.; Frankenberg, C.; Magney, T.S.; Hurlock, S.C.; Seibt, U.; Stutz, J. PhotoSpec: A new instrument to measure spatially distributed red and far-red Solar-Induced Chlorophyll Fluorescence. *Remote Sens. Environ.* **2018**, *216*, 311–327. [CrossRef]

38. Liu, X.J.; Liu, L.Y.; Hu, J.C.; Guo, J.; Du, S.S. Improving the potential of red SIF for estimating GPP by downscaling from the canopy level to the photosystem level. *Agric. For. Meteorol.* **2020**, *281*, 107846. [CrossRef]

39. Zhu, X.D.; Hou, Y.W.; Zhang, Y.G.; Lu, X.L.; Liu, Z.Q.; Weng, Q.H. Potential of Sun-Induced Chlorophyll Fluorescence for Indicating Mangrove Canopy Photosynthesis. *J. Geophys. Res. Biogeosci.* **2021**, *126*, e2020JG006159. [CrossRef]

40. Yang, J.C.; Magney, T.S.; Albert, L.P.; Richardson, A.D.; Frankenberg, C.; Stutz, J.; Grossmann, K.; Burns, S.P.; Seyednasrollah, B.; Blanken, P.D.; et al. Gross primary production (GPP) and red solar induced fluorescence (SIF) respond differently to light and seasonal environmental conditions in a subalpine conifer forest. *Agric. For. Meteorol.* **2022**, *317*, 108904. [CrossRef]

41. Chen, A.P.; Mao, J.F.; Ricciuto, D.; Xiao, J.F.; Frankenberg, C.; Li, X.; Thornton, P.E.; Gu, L.H.; Knapp, A.K. Moisture availability mediates the relationship between terrestrial gross primary production and solar-induced chlorophyll fluorescence Insights from global-scale variations. *Glob. Chang. Biol.* **2020**, *27*, 1144–1156. [CrossRef] [PubMed]

42. Chen, A.P.; Mao, J.F.; Ricciuto, D.; Lu, D.; Xiao, J.F.; Li, X.; Thornton, P.E.; Knapp, A.K. Seasonal changes in GPP/SIF ratios and their climatic determinants across the Northern Hemisphere. *Glob. Chang. Biol.* **2021**, *27*, 5186–5197. [CrossRef] [PubMed]

43. Yang, P.Q.; van der Tol, C. Linking canopy scattering of far-red sun-induced chlorophyll fluorescence with reflectance. *Remote Sens. Environ.* **2018**, *209*, 456–467. [CrossRef]

44. Zhang, Y.G.; Zhang, Q.; Liu, L.Y.; Zhang, Y.J.; Wang, S.Q.; Ju, W.M.; Zhou, G.S.; Zhou, L.; Tang, J.W.; Zhu, X.D.; et al. ChinaSpec: A Network for Long-Term Ground-Based Measurements of Solar-Induced Fluorescence in China. *J. Geophys. Res. Biogeosci.* **2021**, *126*, e2020JG006042. [CrossRef]

45. Li, X.; Cheng, G.D.; Liu, S.M.; Xiao, Q.; Ma, M.G.; Jin, R.; Che, T.; Liu, Q.H.; Wang, W.Z.; Qi, Y.; et al. Heihe Watershed Allied Telemetry Experimental Research (HiWATER): Scientific Objectives and Experimental Design. *Bull. Am. Meteorol. Soc.* **2013**, *94*, 1145–1160. [CrossRef]

46. Du, S.S.; Liu, L.Y.; Liu, X.J.; Guo, J.; Hu, J.C.; Wang, S.Q.; Zhang, Y.G. SIFSpec: Measuring Solar-Induced Chlorophyll Fluorescence Observations for Remote Sensing of Photosynthesis. *Sensors* **2019**, *19*, 3009. [CrossRef]

47. Meroni, M.; Rossini, M.; Picchi, V.; Panigada, C.; Cogliati, S.; Nali, C.; Colombo, R. Assessing Steady-state Fluorescence and PRI from Hyperspectral Proximal Sensing as Early Indicators of Plant Stress: The Case of Ozone Exposure. *Sensors* **2008**, *8*, 1740. [CrossRef]

48. Liu, S.M.; Xu, Z.W.; Wang, W.Z.; Jia, Z.Z.; Zhu, M.J.; Bai, J.; Wang, J.M. A comparison of eddy-covariance and large aperture scintillometer measurements with respect to the energy balance closure problem. *Hydrol. Earth Syst. Sci.* **2011**, *15*, 1291–1306. [CrossRef]

49. Liu, S.M.; Li, X.; Xu, Z.W.; Che, T.; Xiao, Q.; Ma, M.G.; Liu, Q.H.; Jin, R.; Guo, J.W.; Wang, L.X.; et al. The Heihe Integrated Observatory Network: A Basin-Scale Land Surface Processes Observatory in China. *Vadose Zone J.* **2018**, *17*, 1–21. [CrossRef]

50. Lasslop, G.; Reichstein, M.; Papale, D.; Richardson, A.D.; Arneth, A.; Barr, A.; Stoy, P.; Wohlfahrt, G. Separation of net ecosystem exchange into assimilation and respiration using a light response curve approach: Critical issues and global evaluation. *Glob. Chang. Biol.* **2010**, *16*, 187–208. [CrossRef]

51. Meroni, M.; Rossini, M.; Guanter, L.; Alonso, L.; Rascher, U.; Colombo, R.; Moreno, J. Remote sensing of solar-induced chlorophyll fluorescence: Review of methods and applications. *Remote Sens. Environ.* **2009**, *113*, 2037–2051. [CrossRef]

52. Meroni, M.; Busetto, L.; Colombo, R.; Guanter, L.; Moreno, J.; Verhoef, W. Performance of Spectral Fitting Methods for vegetation fluorescence quantification. *Remote Sens. Environ.* **2010**, *114*, 363–374. [CrossRef]

53. Damm, A.; Guanter, L.; Paul-Limoges, E.; van der Tol, C.; Hueni, A.; Buchmann, N.; Eugster, W.; Ammann, C.; Schaepman, M.E. Far-red sun-induced chlorophyll fluorescence shows ecosystem-specific relationships to gross primary production: An assessment based on observational and modeling approaches. *Remote Sens. Environ.* **2015**, *166*, 91–105. [CrossRef]

54. Paul-Limoges, E.; Damm, A.; Hueni, A.; Liebisch, F.; Eugster, W.; Schaepman, M.E.; Buchmann, N. Effect of environmental conditions on sun-induced fluorescence in a mixed forest and a cropland. *Remote Sens. Environ.* **2018**, *219*, 310–323. [CrossRef]

55. Zhang, Y.; Guanter, L.; Berry, J.A.; van der Tol, C.; Yang, X.; Tang, J.; Zhang, F. Model-based analysis of the relationship between sun-induced chlorophyll fluorescence and gross primary production for remote sensing applications. *Remote Sens. Environ.* **2016**, *187*, 145–155. [CrossRef]

56. Gu, L.H.; Han, J.M.; Wood, J.D.; Chang, C.Y.; Sun, Y. Sun-induced Chl fluorescence and its importance for biophysical modeling of photosynthesis based on light reactions. *New Phytol.* **2019**, *223*, 1179–1191. [CrossRef]

57. Liu, L.Y.; Liu, X.J.; Hu, J.C.; Guan, L.L. Assessing the wavelength-dependent ability of solar-induced chlorophyll fluorescence to estimate the GPP of winter wheat at the canopy level. *Int. J. Remote Sens.* **2017**, *38*, 4396–4417. [CrossRef]

58. Joiner, J.; Yoshida, Y.; Guanter, L.; Middleton, E.M. New methods for retrieval of chlorophyll red fluorescence from hyperspectral satellite instruments: Simulations and application to GOME-2 and SCIAMACHY. *Atmos. Meas. Tech.* **2016**, *9*, 3939–3967. [CrossRef]

59. Verrelst, J.; van der Tol, C.; Magnani, F.; Sabater, N.; Rivera, J.P.; Mohammed, G.; Moreno, J. Evaluating the predictive power of sun-induced chlorophyll fluorescence to estimate net photosynthesis of vegetation canopies: A SCOPE modeling study. *Remote Sens. Environ.* **2016**, *176*, 139–151. [CrossRef]

60. Kautsky, H.; Appel, W.; Amann, H. Chlorophyll fluorescence and carbon assimilation. Part XIII. The fluorescence and the photochemistry of plants. *Biochem. Z.* **1960**, *332*, 277–292.

61. Romero, J.M.; Cordon, G.B.; Lagorio, M.G. Re-absorption and scattering of chlorophyll fluorescence in canopies: A revised approach. *Remote Sens. Environ.* **2020**, *246*, 111860. [CrossRef]

62. Govindjee; Papageorgiou, G.C. *Chlorophyll a Fluorescence: A Signature of Photosynthesis*; Springer: Dordrecht, The Netherlands, 2004.

63. Liu, X.J.; Guanter, L.; Liu, L.Y.; Damm, A.; Malenovský, Z.; Rascher, U.; Peng, D.L.; Du, S.S.; Gastellu-Etchegorry, J.-P. Downscaling of solar-induced chlorophyll fluorescence from canopy level to photosystem level using a random forest model. *Remote Sens. Environ.* **2019**, *231*, 110772. [CrossRef]

64. Chen, J.; Shen, M.G.; Kato, T. Diurnal and seasonal variations in light-use efficiency in an alpine meadow ecosystem: Causes and implications for remote sensing. *J. Plant Ecol.* **2009**, *2*, 173–185. [CrossRef]

65. Qiu, R.; Han, G.; Ma, X.; Sha, Z.; Shi, T.; Xu, H.; Zhang, M. CO_2 Concentration, A Critical Factor Influencing the Relationship between Solar-induced Chlorophyll Fluorescence and Gross Primary Productivity. *Remote Sens.* **2020**, *12*, 1377. [CrossRef]

66. Qiu, R.; Han, G.; Ma, X.; Xu, H.; Shi, T.; Zhang, M. A Comparison of OCO-2 SIF, MODIS GPP, and GOSIF Data from Gross Primary Production (GPP) Estimation and Seasonal Cycles in North America. *Remote Sens.* **2020**, *12*, 258. [CrossRef]

67. Liu, X.J.; Liu, L.Y.; Hu, J.C.; Du, S.S. Modeling the footprint and equivalent radiance transfer path length for tower-based hemispherical observations of chlorophyll fluorescence. *Sensors* **2017**, *17*, 1131. [CrossRef]

68. Badgley, G.; Field, C.B.; Berry, J.A. Canopy near-infrared reflectance and terrestrial photosynthesis. *Sci. Adv.* **2017**, *3*, e1602244. [CrossRef]

69. Liu, L.; Liu, X.; Chen, J.; Du, S.; Ma, Y.; Qian, X.; Chen, S.; Peng, D. Estimating maize GPP using near-infrared radiance of vegetation. *Sci. Remote Sens.* **2020**, *2*, 100009. [CrossRef]

70. Zeng, Y.; Chen, M.; Hao, D.; Damm, A.; Badgley, G.; Rascher, U.; Johnson, J.E.; Dechant, B.; Siegmann, B.; Ryu, Y.; et al. Combining near-infrared radiance of vegetation and fluorescence spectroscopy to detect effects of abiotic changes and stresses. *Remote Sens. Environ.* **2022**, *270*, 11285. [CrossRef]